Annual radio frequency identification (RFID) bed particle displacements and morphological development in a wandering gravel-bed river

R. McQueen[1], P. Ashmore[2], T. Millard[1], and N. Goeller[3]

[1]British Columbia Ministry of Forests, Lands, Natural Resource Operations and Rural Development, Nanaimo, BC, Canada, [2]Department of Geography, The University of Western Ontario, London, Ontario, Canada, [3]British Columbia Ministry of Environment and Climate Change Strategy, Victoria, BC, Canada

Corresponding author: Ryan McQueen (rmcquee4@uwo.ca)

Key Points:

- Bed particle displacements reflects both morphologic controls and differences in the annual flow regime
- Bed particle transport and burial is directly tied to patterns of bar-scale erosion and deposition
- The primary mode of tracer deposition was focused along bar margins, primarily at or downstream of the first downstream bar apex

Abstract

Bed particles were tracked using passive integrated transponder (PIT) tags in a wandering reach of the San Juan River, British Columbia, Canada, to assess particle movement around three major bars in the river. In-channel topographic changes were monitored through repeat Lidar surveys during this period and used in concert with the tracer dataset to assess the relationship between particle displacements and changes in channel morphology, specifically, the development and re-working of bars. This has direct implications for virtual velocity and morphologic based estimates of bedload flux, which rely on accurate estimates of the variability and magnitude of particle path lengths over time. Tracers were deployed in the river at three separate locations in the Fall of 2015, 2016, 2017 and 2018, with recovery surveys conducted during the summer low-flow season the year after tracer deployment and multiple mobilising events. Overall, 76 % of the 1399 tracers were recovered. Tracers exhibited path length distributions reflective of both morphologic controls and year to year differences related to the annual flow regime. Annual tracer transport was restricted primarily to less than one riffle-pool-bar unit, even during years with a greater number of peak floods and flow volume exceeding the threshold discharge for bed mobility. Tracer deposition and burial was focused along bar margins, particularly at or downstream of the bar apex, reflecting the downstream migration and lateral bar accretion observed on DEMs of difference. This highlights the fundamental importance of bar development and re-working underpinning bedload transport processes in bar-dominated channels.

1 Introduction

In gravel-bed rivers there is a natural feedback between channel morphology and bedload transport whereby the morphology of the channel is developed through the movement and deposition of individual bed particles and in turn the spatial patterns of bed material transport are controlled at least in part by the morphology of the channel (Church, 2006; Church and Ferguson, 2015). Therefore, attempts at calculating bed material transport rates, or more generally in studying bedload processes, need to consider morphologic controls on bed particle dynamics. This is particularly relevant when employing the virtual velocity approach to estimating bedload flux because it relies upon an accurate measure of the distribution and variability of particle path lengths (travel distances), which may differ greatly in channels of different morphology (Ashmore and Church, 1998; Vázquez-Tarrío et al., 2018).

One idea suggested by Neill (1987), is that bed particle path lengths may be related to, and inferred directly from, the channel morphology. Depositional features such as bars are self-formed through individual particle displacements, so it follows that over the long-term the predominant particle path lengths must be related to the scale and spacing of the bars. This idea is appealing because with sufficient data tying particle path length and burial with the morphological development of bars, it may eventually allow path length to be estimated from morphology without the need for time-consuming and resource intensive direct particle tracking. However, evidence from field-based studies to support the link between bar morphology and particle path length is currently weak.

Throughout the bedload tracking literature, the idea that hydraulic forcing is the primary control on particle transport is prevalent, and functional relationships between average particle travel distances and the combination of flow strength (e.g. Hassan et al., 1992; Phillips and Jerolmack, 2014) and/or grain size (e.g. Church and Hassan, 1992; Wilcock, 1997) have been developed. Many tracer studies, however, have noted differences between path length distributions and theoretical models because of tracers accumulating at distinct regions related to the river morphology (e.g. Bradley and Tucker, 2012). One example of this is the tendency of tracers to be preferentially transported to and stored in gravel bars in channels with riffle-pool-bar morphologies, especially over longer time-scales (Ferguson et al, 2002; Haschenburger, 2013).

In a literature review and re-analysis of published tracer data, Pyrce and Ashmore (2003b) found that the positively skewed path length distributions consistently reported in the literature occurred during moderate discharge events or in smaller channels lacking well-developed sedimentary structures or bar morphology. However, they found that in bar-dominated channels, high magnitude flows (i.e. those capable of altering or forming bars) lead to bi- or multi-modal distribution related to the location of bars. Pyrce and Ashmore's (2003b) flume experiments of an alternate bar channel aligned with these findings, as the authors demonstrated that during bar-forming flows most tracers were deposited on the first bar downstream from the upstream pool in which particles were seeded. Only during lower flows at the critical discharge for gravel entrainment, were positively skewed distributions, with path lengths shorter than bar spacing, observed. Using the same tracer dataset, Pyrce and Ashmore (2005) showed that during bar formation and development bed particle path lengths are commensurate with the spacing of erosion and depositional sites, and that deposition locations tied to bar development processes. In another flume experiment, Kasprak et al. (2015) demonstrated that tracer path lengths were closely related to erosional and depositional processes associated with bar development in a braided channel, with average path lengths on the scale of confluence-diffluence spacing. Similar results have been yielded from more recent modeling of braided channels (Peirce, 2017; Middleton et al., 2019). The question remains however, as to whether these observations are seen in full-scale rivers where conditions are less controlled.

In a synthesis and re-analysis of previously published field-based tracer data, Vázquez-Tarrío et al. (2018) explored the influence of both hydraulic and morphologic controls on particle transport for a range of channel types. They noted that there was a weak positive correlation between stream power and average travel distance for the dataset. However, when travel distance was scaled by a morphological length scale for each channel type (i.e. the spacing between macroscale bedforms), the scatter in the relationship was reduced, indicating that tracer transport has some dependence on channel morphology. Furthermore, analyses of empirical predictors of path length have pointed toward channel width as the most significant control on travel distance (Beechie, 2001; Vázquez-Tarrío and Batalla, 2019). For bar-dominated channels, this may imply that bar spacing exerts a control on path length because the longitudinal spacing of bars is proportional to channel width. These analyses are the starting point to investigating the relationship between path length, bar development and channel scale, but currently this lacks tracer-based data collected in larger bar-dominated channels where morphologic control is expected to be most significant. Therefore, there remains uncertainty as to whether the principles of bed particle dynamics and statistics of displacements, derived from smaller rivers, such as step-pool, plane-bed and low amplitude pool-riffle channels (Montgomery and Buffington, 1997), are applicable to bar-dominated channels with more complex morphology and higher rates of morphological change, and further, if spatial patterns of tracer deposition and burial are tied to bar development.

The paucity of tracer data collected in larger rivers may be explained in part by logistical challenges in searching such large areas of channel, and the potentially deep burial of tracers resulting in low recovery rates. One solution that is increasingly being used to track bed particle movement in larger channels, is the use of passive integrated transponder (PIT) tags (Hassan and Bradley, 2017). PIT tags are small, glass, cylindrical capsules that operate using radio frequency identification (RFID) technology. Several factors make PIT tags an effective technology for bedload tracking including their long lifespan, resistance to abrasion and breakage (Cassel et al., 2017), and the ability to distinguish individual particles from one another using unique codes. Furthermore, as smaller PIT tags are being developed, an increasingly wide range of sediment sizes can be tracked (Hassan and Roy, 2016). Technological improvements in PIT tag technology, such as the increased read range of antennas (Arnaud et al., 2015), innovative surveying strategies (Arnaud et al., 2017) and the development of “wobblestones” (Papangelakis et al., 2019), have made it more possible to track bed particle movement in larger rivers.

The applicability of PIT tags in larger rivers was first explored by Rollet et al. (2008) on the Ain River, France, wherein they recovered 36 % of deployed tracers after one year. More recently, Chapuis et al. (2015) achieved a recovery rate of 40 % on the Durance River, France, while Arnaud et al. (2017) recovered between 11 and 43 % of their tracers over multiple surveys across four years on the Old Rhine, Switzerland. In 2019, Brenna et al. recovered 45 % of PIT tag tracers over a 17 month period on the Parma River, Italy, with recovery rates upward of 80 % for surveys after individual events. However, PIT tags were deployed on less active portions of the channel in Brenna et al.’s study, such as bars and secondary channels, due to difficulties in installing and recovering tracers in the main channel. Overall, deep burial of tracers (beyond the detection range of the antenna used) and tracers being exported downstream of the surveyed reach likely explain most of the loss of tracers in these studies, though it is unclear to what extent each of these factors contributes individually. These studies have yielded promising early results and have provided a template for experimental and equipment design for PIT tag tracking in large rivers, yet the low recovery rates indicate that there is room for improvement.

The primary objective of this study was to explore the relationship between channel morphology and particle path lengths in a large, wandering gravel bed river – the San Juan River, British Columbia, Canada. If the previously observed connection between bar dynamics and particle movement can be established in a field setting it will help support the idea that some information on particle path lengths may be inferred from river morphology. In bar-dominated rivers this would mean that bar spacing may give an approximate long-term average transport distance for morphologic-based calculations of bedload flux. If path lengths are tied to morphology in bar-dominated channels, then particle displacements and burial should be tied to patterns of morphological change over a defined period. To address this objective, PIT tags were used to track bed particle movements and repeat Lidar surveys were conducted to measure morphologic change and bar development during the tracer monitoring period. Combining tracers with morphologic change captured at high resolution is uncommon in the literature and allows a more comprehensive interpretation of the process-form coupling of bedload transport and channel morphology than can be achieved via either method separately.

2 Materials and Methods

2.1 Study Site

The San Juan River, also known by its native name, the Pacheedaht, is located on southern Vancouver Island, British Columbia and drains an area of about 730 km2 (Figure 1a). The main channel is over 50 km long with a total relief of 690 m. The San Juan River valley follows a major east-west fault with distinct topography and bedrock geology on the north and south sides. Bedrock north of the river consists of a series of volcanic and intrusive units, whereas the south side of the valley is underlain almost exclusively by metamorphic rocks of the Leech River Complex (BCGS, 2019). The river outlets to the Strait of Juan de Fuca, near the town of Port Renfrew (Figure 1a).

Forest harvesting in the San Juan River Watershed dates back to the early 1900’s and has been linked to changes in physical habitat and channel morphology in the mainstem and tributaries (NHC Ltd., 1994). This study was guided by watershed management objectives, to provide detailed information on the current sediment dynamics and morphologic changes in the San Juan River which will help inform future restoration decision making.

The study focused on the lower alluvial reach of the San Juan River beginning near Red Creek, downstream of a canyon reach (Figure 1b). The alluvial channel exhibits a wandering morphology, as defined by Mollard (1973) and Neill (1973), with an active width varying between 50-150 m and a reach-averaged slope of 0.0011. During low-flows the river has a single identifiable main channel though it displays a multi-channel pattern during higher-flows when secondary channels are active. Riffle-pool-bar sequences are the primary macroscale bedforms in the alluvial reach, with bars typically on the order of several hundred metres long and up to 100 m wide. Bars are composed primarily of gravel, cobble and sand and there is a general trend of downstream fining of surface sediment calibre both within and between bars. For referencing purposes, mainstem bars were numbered, with Bar 1 being the farthest upstream and subsequent bars numbered in ascending order downstream. Particle tracking focused on Bars 6, 7 and 15, the most accessible sites along the river (Figure 1b).

The closest gauging station to the study sites is the Water Survey of Canada hydrometric station 08HA010, which is installed on the lower San Juan River, approximately 2.5 km downstream from Bar 15 and 7.5 km from Bar 6 (Figure 1b). The 2-, 10-, and 100-year floods are approximately 800, 1050 and 1200 m3/s respectively, though the upper end of the rating curve is uncertain due to the difficulty of obtaining discharge measurements during peak floods. Mean monthly discharge varies from a high of 97 m3/s in January to a low of 4.5 m3/s in August, with a mean annual discharge of 49 m3/s (WSC, 2019). The discharge regime closely follows the seasonal trend in rainfall because 99 % of annual precipitation at low elevations falls as rain (ECCC, 2019), with only transient snow accumulations (no seasonal snowpack) at higher elevations within the watershed.

Figure 1. Location of **(a)** the San Juan River watershed and **(b)** study sites for tracer monitoring.

2.2 Tracer stone deployment and tracking

Half duplex low-frequency (134.2 kHz) PIT tags were inserted into individual gravel bed particles to track annual particle movements around three major bars in the San Juan River. Low-frequency tags are ideal for tracking in coastal and fluvial environments because their signal can pass through water and can penetrate most non-metallic objects (sediment, wood, etc.) better than high and ultra-high frequency tags (Chapuis et al., 2014; Schneider et al., 2010). In 2015, 100 tracers were installed along a cross-section at the head of Bar 6, while between 2016-2018 a further 1199 tracers were installed across the three study sites (Bars 6, 7, and 15) with between 125-142 tracers per site annually. A combination of 12, 23, and 32 mm long PIT tags were used in the original 2015 deployment. However, by 2017 only the 32 mm tags were used because of their larger read range (Chapuis et al., 2014) and higher recovery rates during the first recovery survey.

Wolman particle size counts were conducted at each site to characterize the size distribution of surficial bed material (Wolman, 1954). Native stones were then collected from the San Juan River and brought back to the lab for preparation, which included drilling a cavity in each particle, inserting and epoxying an RFID tag in place, and painting the stone (similar to methods to described in Eaton et al., 2008) Particles were selectively chosen to reflect the size distribution of bed surface material in the channel as best as possible (Figure 2). However, PIT tags did not fit into particles smaller than 22 mm, thus the fine end of the bed material distribution was not well represented. The use of 32 mm tags in 22-32 mm particles biased the size distribution to those with an a-axis longer than 35 mm.

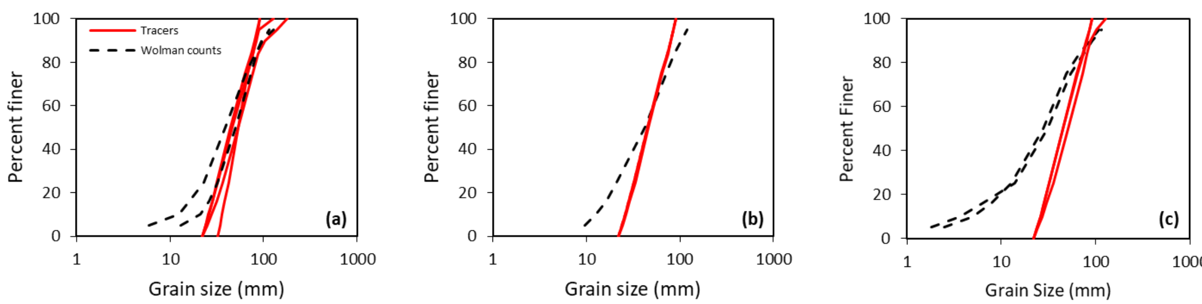

Figure 2. Grain size distributions for surface bed-material and tracers for **(a)** Bar 6, **(b)** Bar 7, and **(c)** Bar 15.

Tracers were deployed annually in the fall, prior to winter flooding, along launch lines perpendicular to the direction of flow. Each launch line spanned the bar head, riffle, and tail of the opposite (upstream) bar, providing the opportunity to observe tracer dispersion around major bars, and to observe differences in particle mobility and path lengths across different morphologic units. While particle path lengths are unlikely to be influenced by seeding position across the channel cross-section in smaller, plane-bed type streams, it has been shown to play a significant role in particle movement in riffle-pool channels with well-developed bar morphology (Liébault et al., 2012). Clusters of tracers were deployed at one to two metre intervals along the launch line by replacing particles on the surface of the riverbed with tracer stones to mimic natural positions and local bed texture. While tracers starting on the surface of the riverbed are more exposed to flow than buried or locked particles, it is not expected that this induced a significant bias on travel distances in this study because multiple floods occurred between deployment and recovery surveys each year, and the timing of discharge events was such that more moderate floods preceded the highest discharge events each year and likely integrated tracer particles into the riverbed prior to the events expected to do most of the work in mobilising bed material.

Tracer recovery surveys were conducted annually during the low-flow seasons at the end of July through August for 2016 to 2019. All recovered tracers were removed from the channel and redeployed at their original launch line the following fall so that each year the deployment strategy was a repeat of the previous one. The winter storm season with several mobilizing flows is treated as an annual event producing annual particle displacements in relation to morphology. This allowed us to assess the morphologic influence on tracer displacements through repeat tests. This decision was also influenced by the practicalities of tracking sediment in a large river because tracking after every event would be onerous and leaving tracers in the channel would likely necessitate increasing the downstream extent surveyed every year, which would quickly become untenable in a river of this size. Furthermore, excavating and removing tracers from the channel allowed us to directly measure tracer burial depths which provides valuable information on active layer dimensions and gives context to particle deposition in relation to morphological development. The maximum downstream extent of survey differed for each location, though generally the first two bars downstream of each seeding site were searched. The deepest portions of pools were omitted from the searching process because they were not wadable, even at low-flow.

Two antennas were used to search for tracer stones. A small handheld wand antenna, the ‘BP Plus Portable’, and a larger ‘Cord Antenna System’, both were purchased from BioMark® (Figure 3). Based on testing in the lab, the wand antenna had a maximum read range around 40-50 cm for the 32 mm PIT tags, though the tag signals are anisotropic, and the read range was as low as 10 cm for certain orientations. The wand antenna was used as the sole antenna for tracer recovery in 2016, resulting in a low recovery rate (33 %), and was used only as a supplementary tool to the larger antenna for subsequent years. Since PIT tag signals interfere with one another when in close proximity (Lamarre et al., 2005; Chapuis et al. 2014), the wand antenna was still a useful tool for distinguishing between PIT tags in areas where tracers were densely concentrated - typically the launch line, as a fraction of the tracer population remained immobile. The wand antenna was also effective for refining the position of tracers after detection with the cord antenna.

The cord antenna system consisted of the cord antenna cable, secured to a 15’ x 5’ (5 m x 1.5 m) rectangular PVC pipe frame, mounted to a backpack frame using a series of ropes, pulleys and cams (Figure 3b). The frame held the cable in a (semi-) rigid structure, stabilising the antenna and allowing it to keep a high current. The operator stood in the centre of the rectangle wearing the backpack and could manipulate the height of each corner of the antenna to help navigate obstacles and changing topography in the field (Figure 3b). The cord antenna covered a much larger surface area than the wand antenna, making it an ideal tool for searching large areas efficiently. It also had a much larger range of detection than the wand antenna, with a maximum read range around 1.75 m, and thus could detect tracer stones buried at greater depths.

Once detected, tracer positions were recorded using one of two methods, and dug up (where possible) to determine a burial depth. For tracers that moved only a short distance (less than 20 m or so), a measuring tape was used to directly measure transport distances from the launch line. For tracers moving larger distances, a handheld Garmin GPS unit was used to record tracer locations. GPS waypoint errors were on the order of two to three metres, which was considered acceptable for the purpose of determining typical particle path lengths, since average path lengths were generally around 100 m, resulting in less than five percent error.

Figure 3. Antennas used during tracer recovery surveys. Panel **(a)** shows the BP Plus Portable wand antenna, and panel **(b)** shows the Cord Antenna System.

2.3 Geomorphic change detection

2.3.1 Topographic surveying

In addition to particle tracking, repeat aerial Lidar surveys, flown by Terra Remote Sensing Inc. in 2015, 2018, and 2019, were contracted for the study and other projects related to management of the river. These surveys were used to generate a series of raster-based digital elevation models (DEMs) of the study sites. Topographic changes between survey dates were then calculated by processing the Lidar DEMs using the Geomorphic Change Detection (GCD) software (Wheaton et al., 2010) to produce DEMs of difference (DoDs). DoDs provided spatial patterns of erosion and deposition between surveys as well as volumetric changes, which when combined with virtual velocity data from the tracer particles can provide a measure of the bed material flux through each site.

Each Lidar survey was conducted using the Reigl LMS-1780 sensor from an airborne platform. Ground accuracy tests, performed by Terra Remote Sensing Inc., involved both internal and external horizontal and vertical checks (TRS Inc., 2018a,b, 2019). Internal checks were conducted via comparison of intra- and inter-flight areas of overlap. External checks consisted of two components: comparison of the Lidar ground surface with control stations not used in the calibration process, and with a series of check points collected on open surfaces using Post Processed Kinematic (PPK) GPS. For the 2015, 2018, and 2019 surveys, checks with control points resulted in a vertical root mean square error (RMSEv) of 0.032, 0.026, and 0.007 m for each year respectively. For the 2019 survey, a RMSEv of 0.069 ± 0.062 m was obtained through comparison with 43 check points, though check point accuracy was not reported for the 2015 and 2018 surveys (TRS Inc. 2018a,b, 2019).

Survey point densities were spatially variable across the study sites. Flat, exposed areas such as gravel bars had the highest point densities, while vegetated areas typically had intermediate point densities. Shallow water surfaces (i.e. riffles) had low point densities, and deeper water (i.e. pools) had zero returns in the point cloud because the near-infrared lasers emitted by the sensor were absorbed by the deeper water column. Overall, the 2015 survey had a point density of 12.8 ± 7.2 pulses/m^2, the 2018 survey had a point density of 28 ± 16 pulses/m^2, and the 2019 survey had a point density of 38 ± 11 pulses/m^2.

2.3.2 DEM analysis

The Lidar-derived DoDs (Difference of DEMs between successive surveys) were used to interpret patterns of tracer displacement and burial depths, and to provide information on morphological development of the bars during the study period. They were not used to calculate complete reach-scale sediment budgets due to the lack of in-channel topographic data and stage differences during each Lidar survey affecting the relative portion of the river bed that was exposed. Currently, collecting reach-scale bathymetric data in large channels is challenging and relies on either boat-based multibeam echo sounding (MBES) systems or green wavelength Lidar sensors (Tomsett and Leyland, 2019).

To account for uncertainty in the DEMs, a spatially variable uncertainty analysis was conducted using the GCD ArcMap extension. This involves three main steps: 1) an estimate of uncertainty for each individual DEM; 2) propagation of these errors through the DoD; and 3) an assessment of the statistical significance of these uncertainties in distinguishing real geomorphic change from noise (Wheaton et al., 2010). A major appeal of this method is that it requires little to no additional survey error information other than the survey data itself. Further, accounting for spatially-variable error allows for recovery of information in areas with low elevation uncertainties that would otherwise be lost.

Lidar DEMs were produced at a 10 cm spatial resolution by converting point clouds to a TIN, from which concurrent raster DEMs were generated using linear interpolation. For each DEM, two surfaces were generated for uncertainty analysis using the built-in tools in the GCD software: a point density raster and a slope raster. The rationale behind using these surfaces was that steep areas with low point density have high elevation uncertainty, whereas flat areas with high survey point density will generally have lower elevation uncertainty (Wheaton et al., 2010). These surfaces were then combined on a cell-by-cell basis, using a fuzzy inference system (FIS), to produce an elevation uncertainty surface. Uncertainty surfaces associated with individual DEMs were then combined using simple error propagation (Brasington et al., 2003) to produce a single propagated error surface for the DoD. The GCD software then uses probabilistic thresholding to determine the statistical significance of these uncertainties. The probability that the elevation change associated with each individual cell of the DoD is then assessed at a user-defined confidence interval, in this case 80 %. Originally, 95 % was chosen, however upon examination of output thresholded DoDs, this limit appeared too restrictive, with real change being removed from areas of eroding banks and in obvious areas of deposition.

2.4 Critical discharge estimation

Streamflow data from the WSC hydrometric station was used to calculate the bankfull discharge for the river, which was used as an approximate critical discharge for gravel entrainment. This allowed us to estimate the number and duration of potentially mobilising events each season during the four years of tracer monitoring. A critical discharge (Qc) of 500 m3/s was calculated using the velocity-area approach, using cross-sectional areas at each tracer launch line obtained from Lidar DEMs and average cross-section velocities calculated from appropriate flow resistance equations (Ferguson, 2013). A sensitivity analysis suggested this number is accurate to within ± 100 m3/s. The calculated Qc is an approximation but appears in line with time-lapse imagery of the river during bankfull flows (Figure 4) and provides a relative number to give context to any obvious differences in the tracer path length data between years that might be the result of different mobilizing conditions.

The number of events exceeding the estimated critical discharge, as well as the days of flow above this threshold, total volume of flow above this threshold, and peak instantaneous discharge are summarized in Table 1. The highest discharge events occurred during the winters of 2015-2016 and 2017-2018 in which peak discharges above 1000 m3/s were recorded. These two years also recorded the highest number of floods above the critical discharge (six) and the greatest total volume of competent flow (Table 1). The lowest peak annual discharge and lowest total competent flow volume occurred during the winter of 2016-2017, while intermediate values were recorded for 2018-2019 (Table 1). The hydrograph for the period of the tracer study is presented in Figure 5. This figure illustrates that even if the estimate critical discharge was shifted substantially, say 100 m3/s, the number of mobilising events would change very little. Therefore, the response of tracers to the number of potentially mobilising flows in a season can be meaningfully interpreted, though this was not a primary focus of this study.

Figure 4. Time-lapse imagery of the apex of Bar 6 on **(a)** September 18th, 2017 at 1:45 pm. The hydrometric station recorded a discharge of 1.2 m^3/s at the time of this image. The apex of Bar 6 on **(b)** November 19th, 2017 at 3:45 pm. The hydrometric station recorded a discharge of 560.4 m^3/s at the time of this image.

Table 1. Summary of the San Juan River hydrological regime from 2015 to 2019. $\sum V_{cr}$ is the total flow volume above 500 m^3/s integrated from five-minute interval discharge data at WSC station 08HA010.

Season	# of Threshold Events ($Q > Q_c$)	Days of Competent Flow	$\sum V_{cr}$ (dam^3)	Q_{max} (m^3/s)
2015-16	6	13	41,990	1,022
2016-17	4	8	24,342	749
2017-18	6	15	65,416	1,003
2018-19	5	7	35,201	942

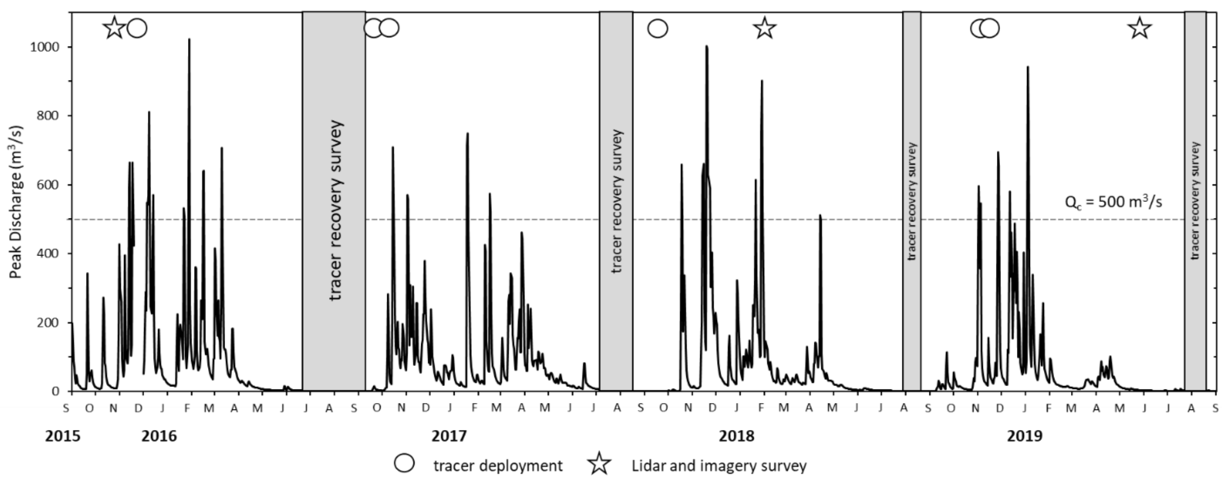

Figure 5. San Juan River hydrograph from September 2015 to September 2019. Data from WSC, 2019.

3 Results

3.1 Tracer recovery rates

Overall, 76 % of the tracers deployed in the river were recovered, with between 70 and 81 % recovered from individual launches (Table 2). Typically, about 65-75 % were recovered during the first survey after tracer deployment, with an additional 5-10 % recovered in surveys two or more years after deployment. Recovered tracers were treated collectively for path length analysis because those recovered more than one year after deployment only comprised a small fraction of the tracer population and the focus of the analysis was on looking at particle deposition and burial in relation to morphology for which these tracers still provide valuable information. The fact that recovery rates were high indicates that few tracers could have been deposited in the deeper portions of the channel (areas not searched during recovery surveys). The one case in which recovery rate was substantially lower than other sites was the original 2015 deployment of tracers at Bar 6, of which 33 % were recovered in the initial survey because only the wand antenna was used to search for tracers in this survey. However, a further 48 % of the tracers were recovered two or more years after deployment using the larger antenna.

Table 2. Summary of tracer recovery rates. Note that n = number of deployed tracers, n_r = number of recovery tracers and recovery rates, r, were calculated as $\sum n_r$ / n.

Location	Year of Deployment	n	$n_{r, 2016}$	$n_{r, 2017}$	$n_{r, 2018}$	$n_{r, 2019}$	$\sum n_r$	r (%)
Bar 6	2015	100	33	43	5	0	81	81
	2016	134	-	88	13	0	101	75
	2017	142	-	-	101	10	111	78
	2018	134	-	-	-	101	101	75
Bar 7	2016	132	-	100	4	0	104	79
	2017	131	-	-	90	8	98	75
	2018	125	-	-	-	99	99	79
Bar 15	2016	134	-	94	3	0	97	72
	2017	136	-	-	88	7	95	70
	2018	131	-	-	-	98	98	75

3.2 Particle displacements

Path length frequency distributions for tracers deployed at Bars 6, 7, and 15 are presented in Figure 6, and maps illustrating the final position of recovered tracers for each site are presented in Figures 7, 8, and 9 respectively. Results from each site are summarized separately in sections 3.2.1. to 3.2.3, then results are compared between sites in section 3.2.4.

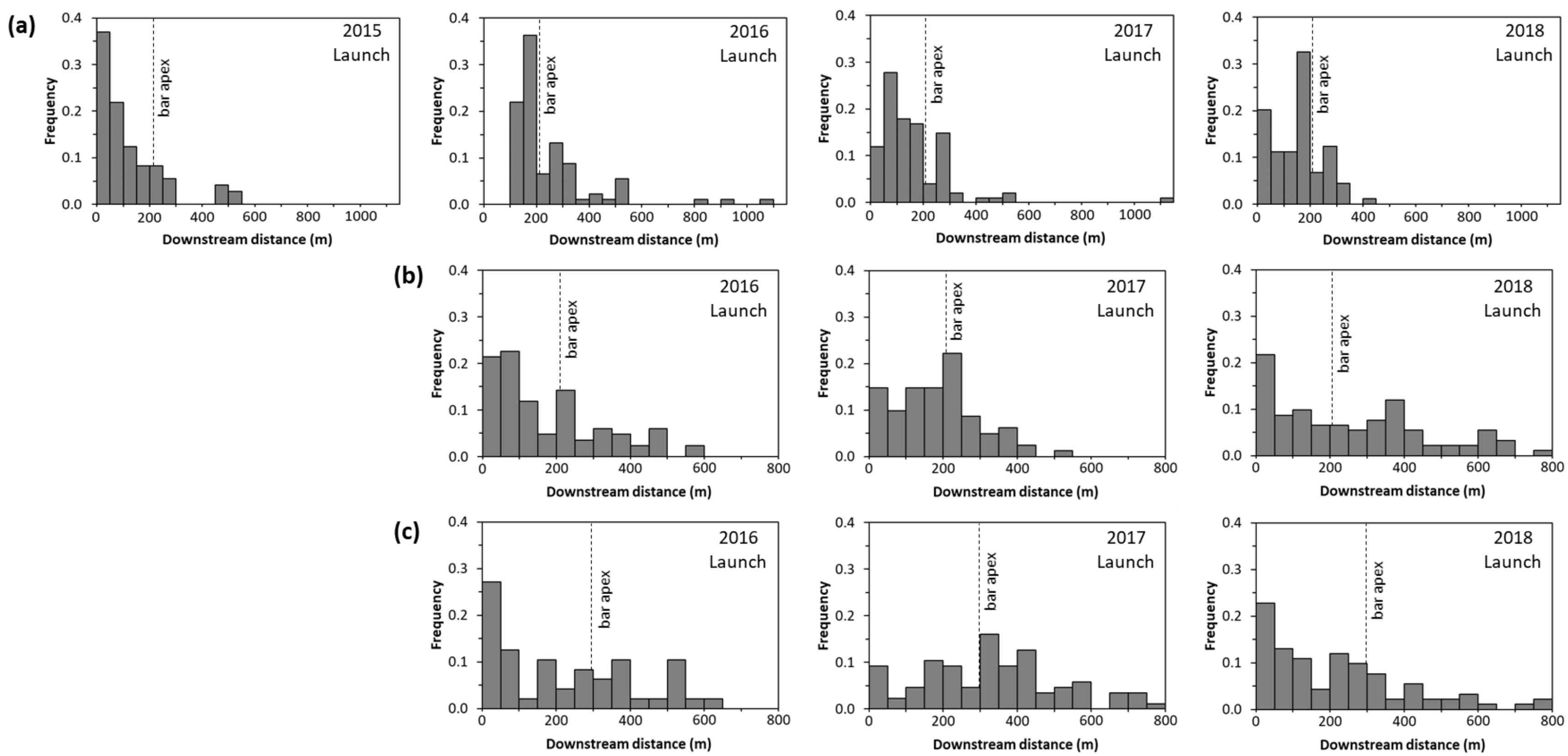

Figure 6. Path length frequency distribution for **(a)** Bar 6, **(b)** Bar 7, and **(c)** Bar 15 mobile tracers (i.e. transported more than 10 m downstream).

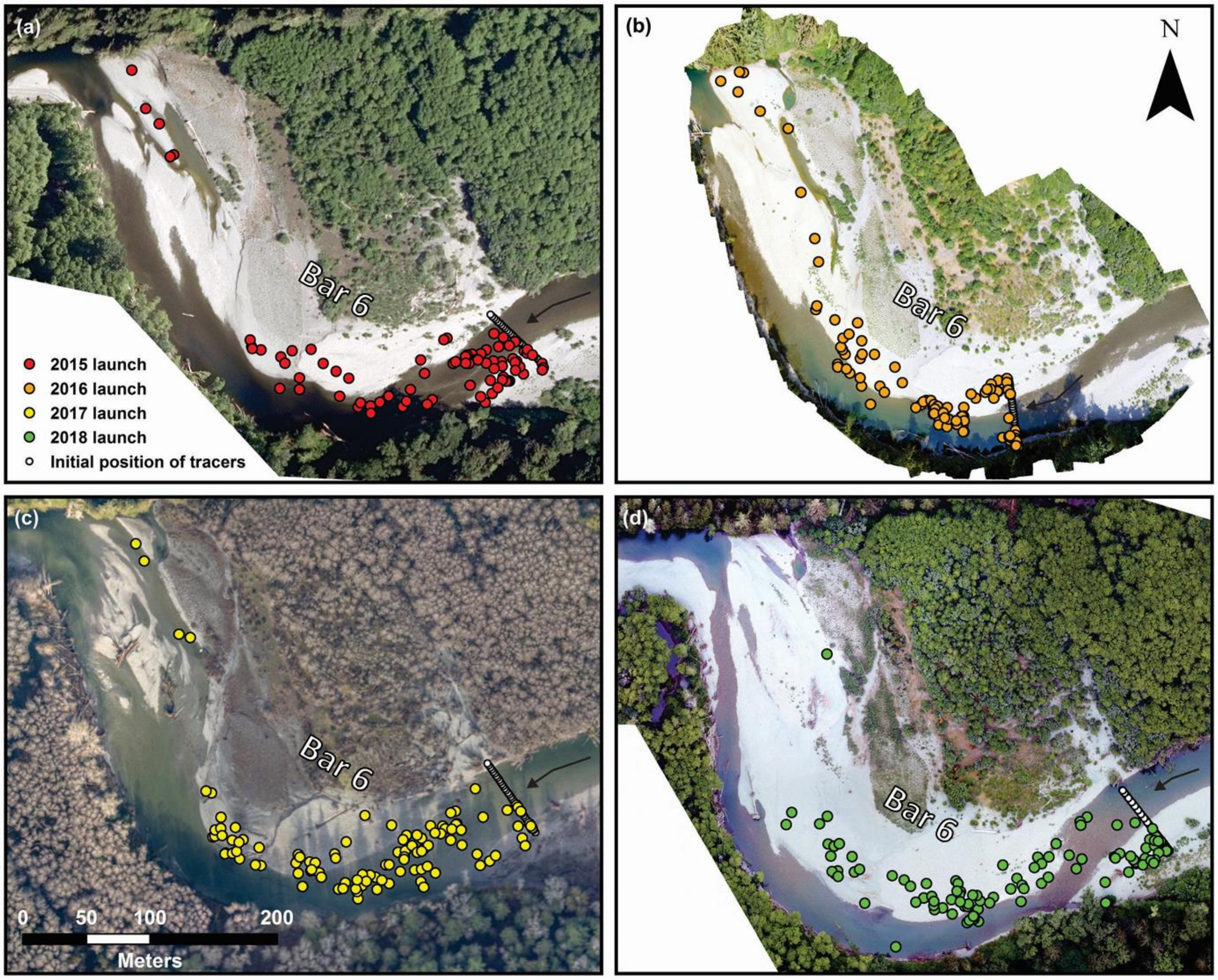

Figure 7. Tracer recovery locations for Bar 6 deployed in **(a)** 2015, **(b)** 2016, **(c)** 2017, and **(d)** 2018.

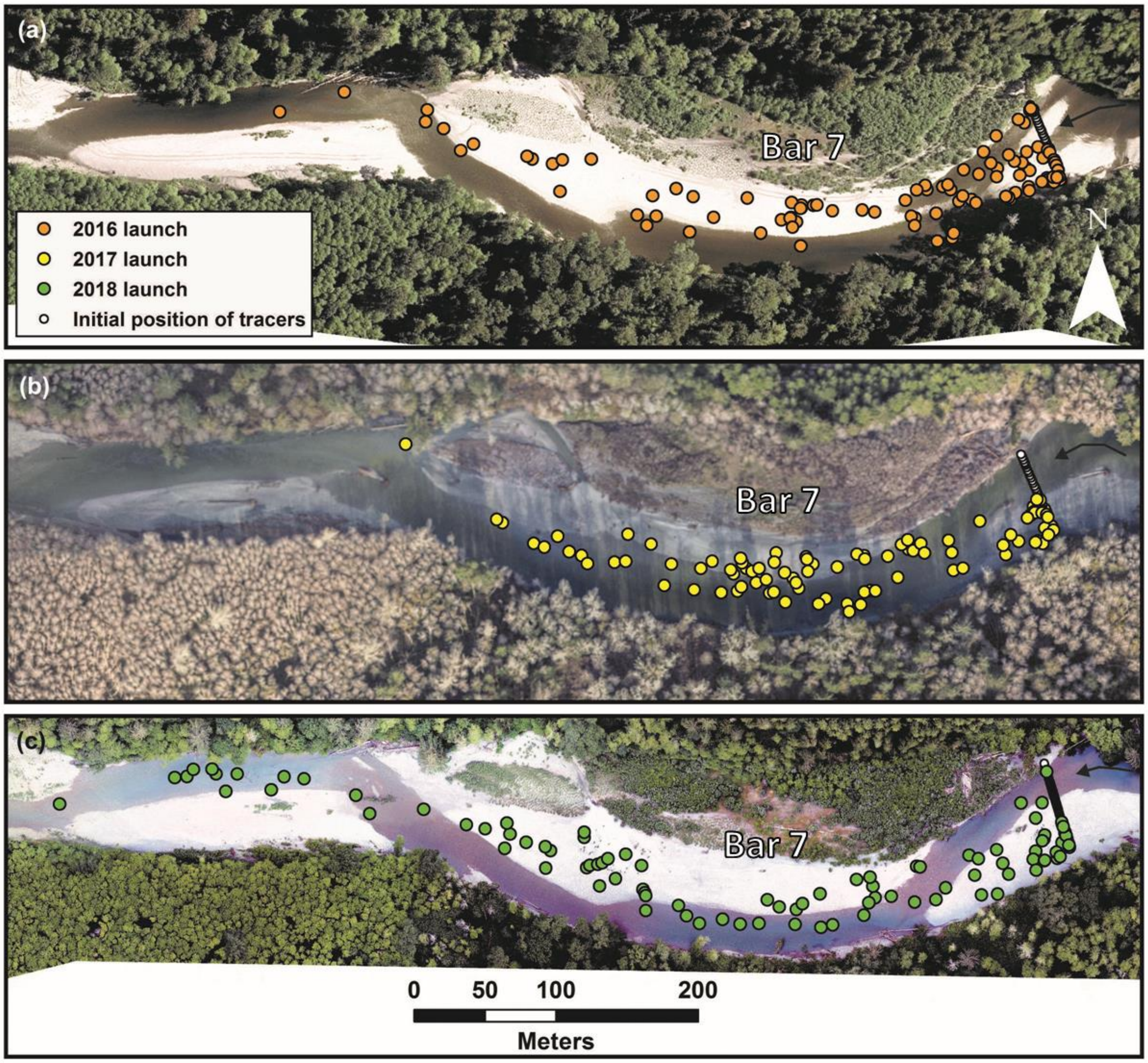

Figure 8. Tracer recovery locations for Bar 7 deployed in **(a)** 2016, **(b)** 2017, and **(c)** 2018.

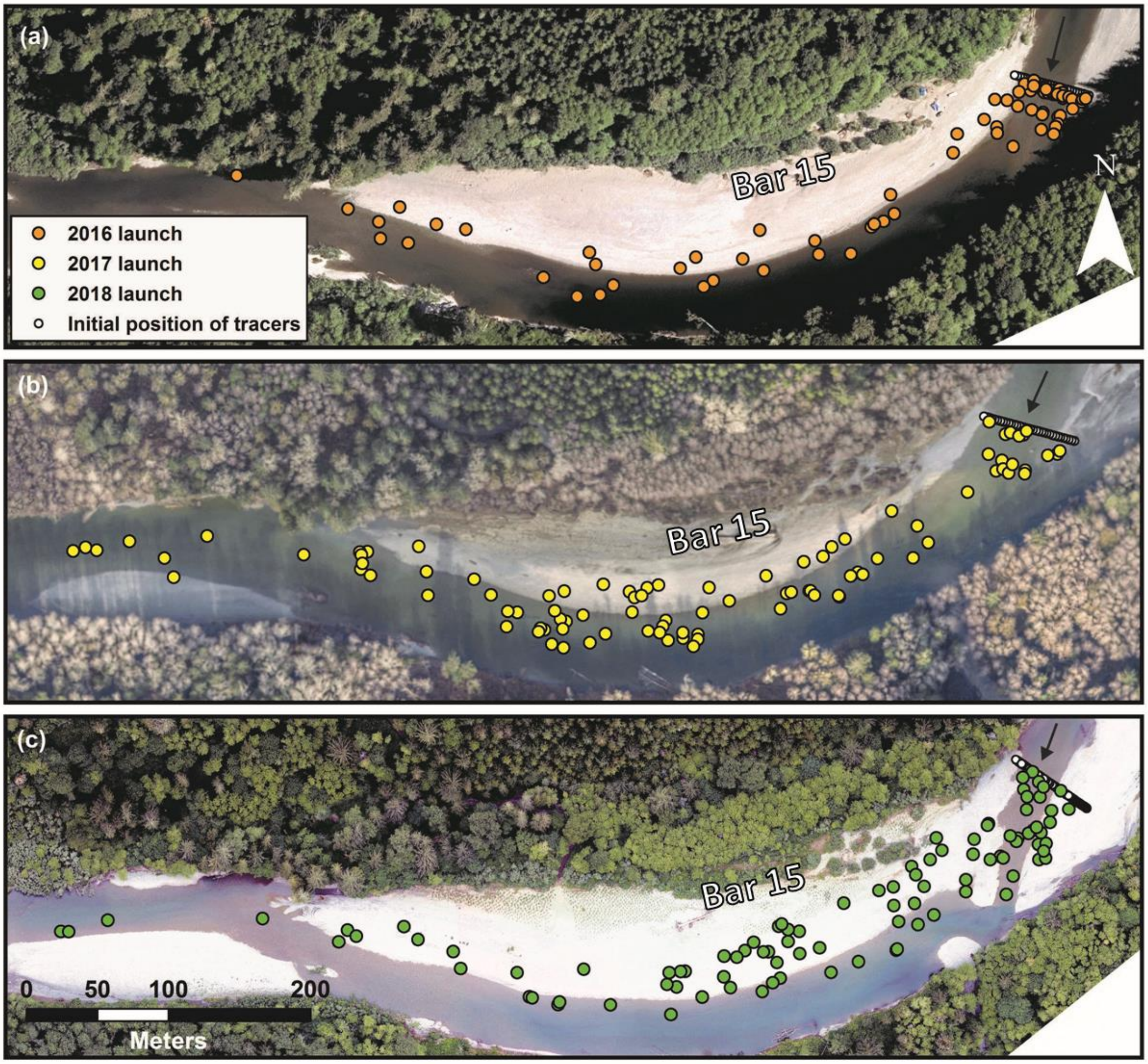

Figure 9. Tracer recovery locations for Bar 15 deployed in **(a)** 2016, **(b)** 2017, and **(c)** 2018.

3.2.1 Bar 6

The Bar 6 launch line was located at the bar head/riffle for 2015, 2017, and 2018 deployments, but was moved 112 m downstream for tracers deployed in 2016 so that tracer displacement out of the pool could be assessed (Figure 7b). To plot the tracer path lengths on a common downstream axis, the upstream launch line was defined as the origin and all data was plotted relative to that point (i.e. 112 m was added to 2016 path lengths). Despite the launch line remaining in the same physical location for 2015, 2017 and 2018, the morphology of the channel appeared to change over time at this cross-section. For the initial deployment of tracers in 2015, this site was the upstream end of a riffle between Bars 5 and 6, however, by 2018 the channel had scoured the area of the launch line and the riffle had migrated downstream. Patterns of tracer movement and deposition appear to have been influenced by this change in the morphology at the launch line. In 2015, tracers clustered primarily within 50 m of the launch line, remaining in the initial riffle (Figure 6a, 7a). In 2017 however, the focus of deposition was 50-100 m downstream of the launch line (Figure 6a, 7b), evidence of the continued downstream translation of the riffle. In 2018, while there was a short-transport mode of tracers, this was caused by the low mobility of tracers seeded on the tail of Bar 5 (Figure 7d). Nearly all tracers that were initially seeded in the low-flow wetted channel were exported downstream of the riffle, with the primary mode of deposition focused on the surface of Bar 6, just upstream of the bar apex (Figure 6a, 7d). For the 2016 deployment, tracers were seeded across a portion of Bar 6 and the adjacent pool (Figure 7b). Tracers seeded on the bar surface tended to remain immobile or only be displaced short distances, while those seeded in the pool were generally transported farther downstream. The year to year differences observed here highlight the importance that deployment strategy and channel morphology can have on tracer dispersion.

Path length distributions for Bar 6 were positively skewed for 2015, 2016, and 2018 deployments, though as previously mentioned the reason for the short-transport mode each year likely varies. The 2018 deployment exhibited a bi-modal distribution, with the primary mode of deposition focused upstream of the bar apex, and the secondary mode related to tracers remaining relatively immobile on the tail of Bar 5 (Figure 6a).

Despite the variation between years, Bar 6 tracer displacements followed some key trends. Tracers deployed on the tail of Bar 5 consistently remained on the bar tail, exhibiting lower mobility and transport relative to tracers seeded closer to the thalweg. Also, there was a consistent clustering of tracers deposited at or near the apex of Bar 6, particularly noticeable in the 2016 and 2018 deployments (Figure 7b,d). This appears to be related to the growth of a coarse gravel sheet, which migrated downstream from the bar head between 2015 and 2019, terminating at the bar apex. Few tracers were transported to the bar tail, and those that did were preferentially deposited along a bar-top channel, visible in the higher-flow orthophotos from 2018 (Figure 7c). In 2016 and 2017 one and two tracers travelled past the bar (not shown in Figure 7a or 7b), otherwise tracer displacement remained within one bar length of the initial seeding site.

3.2.2 Bar 7

In 2016, the Bar 7 path length distribution was positively skewed, with 44 % of recovered tracers located within the first 100 m downstream of the launch line (Figure 6b). In 2017, tracers exhibited greater dispersion. The path length distribution was symmetrical, with deposition focused at the bar apex region. In 2018, the distribution was positively skewed, though there was a minor peak in the distribution, reflective of tracers accumulating on the tail of Bar 7 (Figure 6b). Overall, Bar 7 tracers remained within a single riffle-pool-bar sequence, with 98, 100, and 88 % of tracers located upstream of the tail of Bar 7 for 2016, 2017, and 2018 deployments respectively.

Similar to Bar 6, the morphology at the Bar 7 launch line changed throughout the tracer study. Between 2015 and 2019 an upstream point bar on the inside of the channel bend expanded through a portion of the Bar 7 tracer launch line, affecting the patterns of tracer movement. In 2016, tracers exhibited low mobility across the entire width of the launch line (Figure 8a), likely a result of the flow regime this year, which had the lowest number of potentially mobilising events and peak discharge (Table 1). However, in 2017, only tracers deployed on the south (river left) side of the launch line exhibited low mobility and short transport distances, with tracers seeded closer to the thalweg being exported farther downstream (Figure 8b). This appears to be a response to the growth of the point bar in this area burying tracers (see Section 3.4.1), rendering these particles less likely to be mobilised. A similar pattern was observed in the 2018 deployment, whereby tracers seeded on the point bar tended to remain on the bar tail (Figure 8c).

3.2.3 Bar 15

In 2016, Bar 15 tracer mobilisation was low, as only 51 % of recovered tracers were transported more than 10 m downstream. Mobile tracers exhibited a positively skewed path length distribution, with 37 % of tracers recovered within 50 m of the launch line, mainly in the riffle in which they were seeded (Figure 6c). Of the tracers that were transported downstream of the riffle, deposition focused along the bar-pool margin of Bar 15, and just a single tracer was recovered downstream of the tail of Bar 15 (Figure 9a). In contrast, 2017 tracers exhibited greater overall dispersion. Tracer path lengths followed a symmetrical distribution, with the primary focus of deposition located downstream of the apex of Bar 15 (Figure 6c). Seven tracers from the 2017 deployment (8 % of the recovered population) were recovered downstream of Bar 15 (Figure 9b). In 2018, the tracer path length distribution was positively skewed (Figure 6c), with only three tracers recovered downstream of Bar 15 (Figure 9c).

3.2.4 Summary of particle displacements

For all three sites, a few consistent trends in particle displacements were observed. Tracers seeded on bar tails were largely immobile or only displaced short distances, remaining on the bar tail, whereas those seeded closer to the thalweg were generally transported farther downstream. This highlights the spatially variable nature of bed-material transport in bar-dominated channels. For those tracers that were transferred farther downstream, deposition focused at or around the apex of the first bar downstream, and generally along the bar-pool margin. This reflects lateral bar accretion, typical of wandering channels like the San Juan River. Additionally, tracers were rarely transported more than one bar length downstream, indicating that annual particle transport distances on the San Juan River are typically on the order of one riffle-pool-bar unit.

Tracer displacements were substantially influenced by the annual flow regime. In the winter of 2016-17 the peak instantaneous discharge was lower than other seasons, and there were fewer potentially mobilising floods all together (Table 1). Tracer deployments from this year all exhibited positively skewed path length distributions, with most tracers remaining either completely immobile, or at least remaining within the initial riffle in which they were seeded. During this season, morphologic effects on particle movement are less evident than other years due to lack of mobilisation. In the winter of 2017-18 however, there were larger and more frequent peak discharge events, resulting in greater tracer dispersion. For Bar 7 and Bar 15, tracers exhibited symmetrical path length distributions, with the primary focus of deposition at or downstream of the bar apex. Even with more frequent and larger peak floods, tracer transport was still generally limited to less than one bar-length downstream. In the winter of 2018-19, there were fewer potentially mobilising floods and peak discharge was lower than in 2017-18, but these numbers were greater than in 2016-17. Tracers from 2018-19 exhibited a short-transport mode for all three sites, caused by deposition of fine gravel and sand on the bar tails and over the top of a portion of the launch lines. In addition to the short-transport modes, the highest fraction of tracers being transported more than one bar length occurred during this season, as 12 % of recovered tracers from Bar 7 were located downstream of the bar tail. Overall, tracer displacements showed differences year to year, and reflected both the discharge regime and complicated, local interactions with morphologic change and bar dynamics.

3.3 Grain size effects on path length

In riffle-pool channels, the idea that size-dependent path lengths may arise due to size sorting effects around bars has been suggested by Pyrce and Ashmore (2005) but has since received little attention in the tracer literature. This idea differs from the standard hydraulics-dominated displacements documented in tracer studies from smaller, less dynamic channels (see Figure 6.2 in Hassan and Bradley, 2017). Tracer data from the San Juan River provides the opportunity to investigate size-dependent path lengths related to bar sedimentation and morphology for a bar-dominated channel. A box plot of grain size versus path length is presented for Bars 6, 7, and 15 in Figure 10.

In general, there was an inverse relationship between particle size and path length across the three sites. This trend is most apparent for Bar 15 tracers whereby the median path length for 22-32 mm tracers is 398 m and the median path length for 64-90 mm tracers is just 114 m (Figure 10c). Each size class also exhibited a wide range of path lengths for Bar 15, likely caused, at least in part, by differences in seeding location and annual differences in the flow regime (McQueen, 2019). Like Bar 15, tracers seeded at Bar 7 showed decreasing path length (both median and maximum) with increasing grain size (Figure 10b).

In contradistinction to Bar 15 tracers, Bar 6 tracers exhibited a narrower range of path lengths for each size class, and smaller differences in average path lengths between size classes. A possible explanation for the differences observed between Bar 15 and Bar 6 may be due to local characteristics of each reach. At Bar 6 the channel takes a sharp meander approximately 200 m downstream of the bar head, with high rates of sedimentation on the bar apex in this area (see Section 3.4.1 and Figure 11). Annual tracer displacements downstream of the Bar 6 apex appear to be limited across all grain sizes (Figure 10a), resulting in a lower variation in path lengths for each size class, and smaller differences between average path lengths between size classes.

While the dataset for this study was not collected with the intent to determine size-sorting effects around bars, the cursory analysis here does shed some preliminary insight into the possibility of size-dependent path lengths related to bar-scale deposition. It appears that Bar 15 and to a lesser extent Bar 7 tracers exhibit the more classic style of hydraulics-dominated displacements, whereas path lengths of Bar 6 tracers appear to be more influenced by bar morphology and development. This is relevant because it implies that size-sorting around bars may be an important consideration for developing models of size-dependent transport in bar-dominated channels at least for certain reaches. A more thorough statistical analysis is required to investigate size-sorting effects further, which could include the characterization of spatial variations in the size of bed material across the bar and channel to help provide context to size-dependent tracer deposition and clustering.

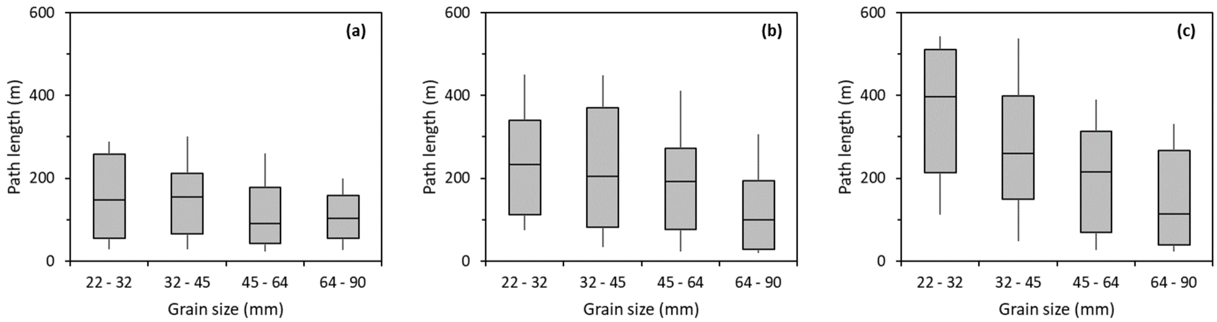

Figure 10. Tracer path length as a function of grain size for **(a)** Bar 6, **(b)** Bar 7, and **(c)** Bar 15. Note that only annual displacements are included in this figure, with any tracers recovered more than one year after deployment removed from this analysis.

3.4 Morphologic change and particle burial

Path length data demonstrated a relation with channel morphology which can be further explored in relation to the geomorphic change detection analysis and incorporating tracer burial depth data.

3.4.1 Bars 6 and 7

In Figure 11, DoDs are presented for 2015-2018 and 2018-2019 for the Bars 6-7 reach with tracer burial depths and locations overlaid on top. Tracers that were recovered on the bed surface were not included. Furthermore, tracers that were located using the cord antenna system but were too deep to be detected by the wand antenna (or physically recovered), were estimated to be deeper than 30 cm (a conservative estimate of the maximum detection range of the wand antenna). Tracers recovered in pools were not physically recovered so burial depth was unknown and they were not included in burial depth analyses.

Overall, a general pattern of downstream channel migration was observed over the period of study. Primary areas of erosion include the heads of Bars 6, 7, the small point bar between Bars 6 and 7, and erosion of the banks opposite the bars. Scour pools also developed along the tail of Bar 6 between 2015 and 2018 (Figure 11). Bar surfaces were net depositional across the DoDs, with maximum deposition focused at the bar apexes and bar tails.

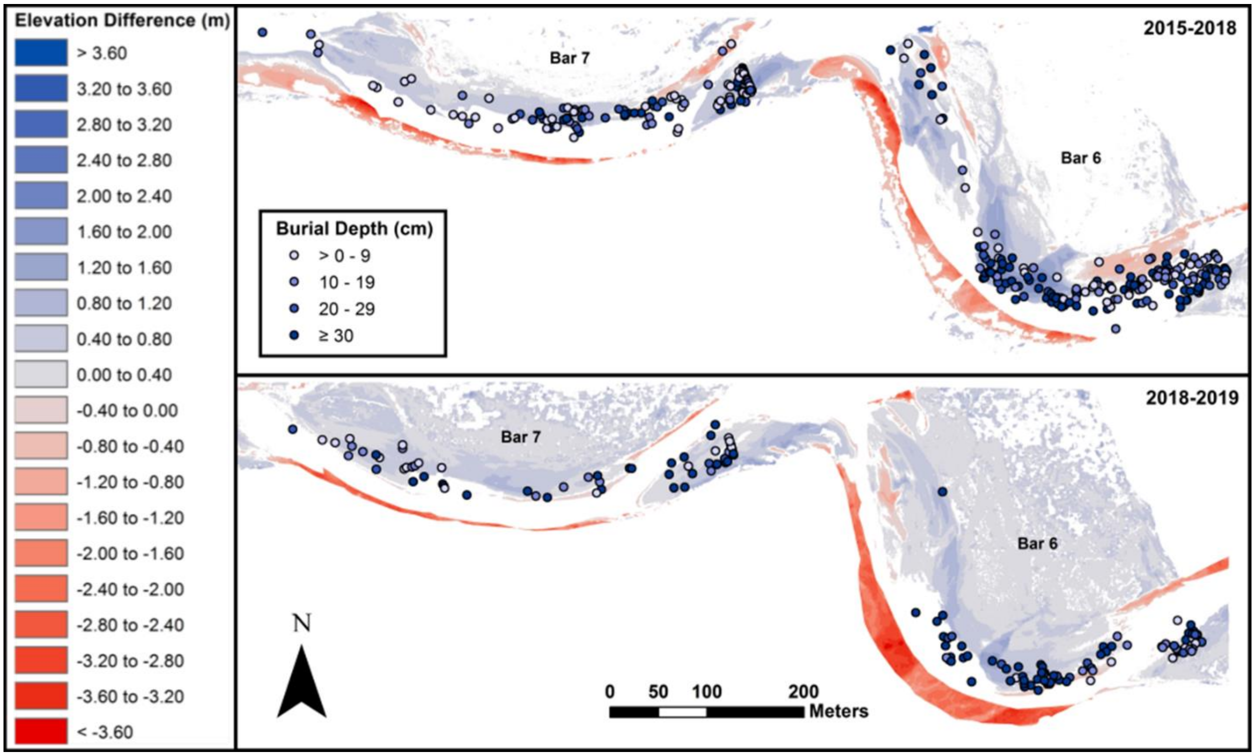

Figure 11. Tracer burial for Bar 6 and Bar 7. The position of buried tracers that were recovered between 2015 and 2018 are overlaid on the corresponding DoD in the upper panel. Those recovered in 2019 are shown in the lower panel overtop of the 2018-2019 DoD.

In general, the spatial pattern of tracer burial was well-reflected in the DoDs. Excluding areas of indeterminate change on the DoDs, 90 % of Bar 6 and Bar 7 buried tracers were recovered in areas of net deposition, with 10 % recovered in areas of net erosion. Areas of indeterminate change were mostly in-channel areas such as riffles and pools. In both 2015-2018 and 2018-2019, maximum tracer burial depths occurred near the apex of Bar 6, aligning with the high deposition detected on the DoDs in this area – which includes the downstream extent of the coarse gravel sheet. Similarly, tracer burial on the tail of Bar 5 (upstream bar opposite Bar 6) and the small point bar between Bars 6 and 7 were reflected as areas of bar accretion in the DoDs (Figure 11). The deep burial of these particles reduces their chance of re-entrainment, until there are future flows capable of eroding this area and remobilising sediment at this depth. In other words, their long-term mobility and travel will be directly tied to the evolution of the bar.

The distribution of tracer burial depths for Bar 6 and Bar 7 is presented in Figure 12a and 12b respectively. The maximum burial depth for Bar 6 tracers was 52 cm, although 34 % of tracers were not physically recovered, and we suspect that they are buried deeper than 30 cm (because they were not detected with the wand antenna) (Figure 12a). Assuming that these tracers were buried beyond this depth, the median burial depth for Bar 6 tracers was 25 cm. A maximum burial depth of 47 cm was recorded for Bar 7 tracers, with 30 % of tracers not physically recovered, likely due to deep burial, and an overall median burial depth of 18 cm (Figure 12b). For both locations, more than 40 % of tracers were recovered at depths exceeding the commonly cited value for the maximum active layer depth of 2 D90 (Haschenburger, 2012; Haschenburger and Church, 1998). Tracer burial data from Bars 6 and 7 suggests that maximum active layer thickness may be 50 cm or greater locally. This indicates that in this type of channel the particle exchange during bed material transport may operate at depths beyond a surface layer a few grains thick for at least a portion of the bed and active layer depth is governed by the distribution of bar-scale erosion and deposition.

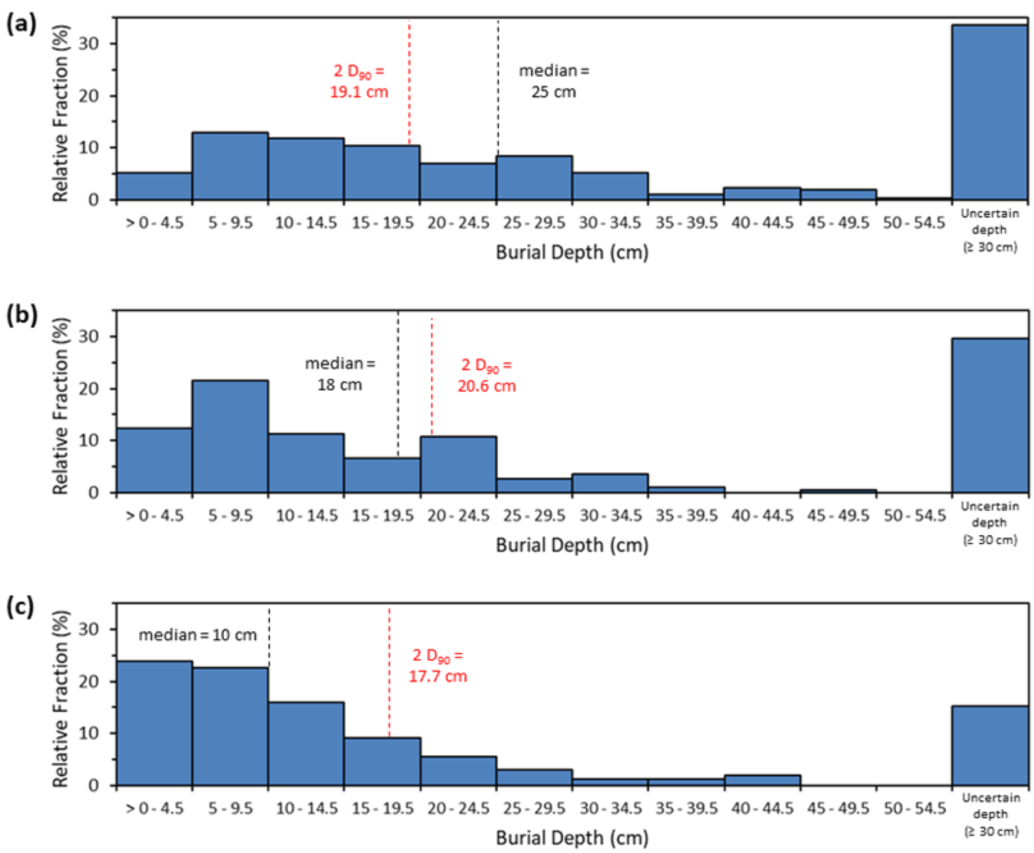

Figure 12. Tracer burial depths for **(a)** Bar 6, **(b)** Bar 7, and **(c)** Bar 15.

3.4.2 Bar 15

In Figure 13, DoDs are presented for 2015-2018 and 2018-2019 for the Bar 15 reach with tracer burial depths and locations overlaid on top. Over the four years of tracer monitoring (2015-2019), the tail of Bar 14 grew substantially, migrating over the left side of the tracer launch line. In turn, the channel scoured the head of Bar 15, leading to an overall downstream migration of the bar, with net deposition over the downstream portion of the bar surface. Maximum deposition occurred downstream of the bar apex for both Bars 15 and 16 from 2015 to 2019. The bank opposite Bar 15 retreated over this period, though at a much lower rate than observed opposite Bar 6.

During the 2015 to 2018 period, tracer burial was particularly shallow relative to the other sites, with few particles buried deeper than 30 cm (Figure 13). From 2018-2019, deeper tracer burial was observed. This was in large part caused by the tail of Bar 14 migrating downstream over a portion of the launch line, resulting in deep burial of tracers seeded in this area (Figure 13). Only 24 % of buried tracer positions overlapped areas of change on the Bar 15

DoDs. This was largely influenced by the lack of topographic data captured for the riffle between Bars 14 and 15, a site where many tracers were buried (Figure 13). Of the tracers that were buried in areas of known net change on DoDs, 72 % were recovered in net depositional areas and 28 % were recovered in net erosional areas, supporting the idea that particle transport and deposition is directly tied to overall channel morphodynamics.

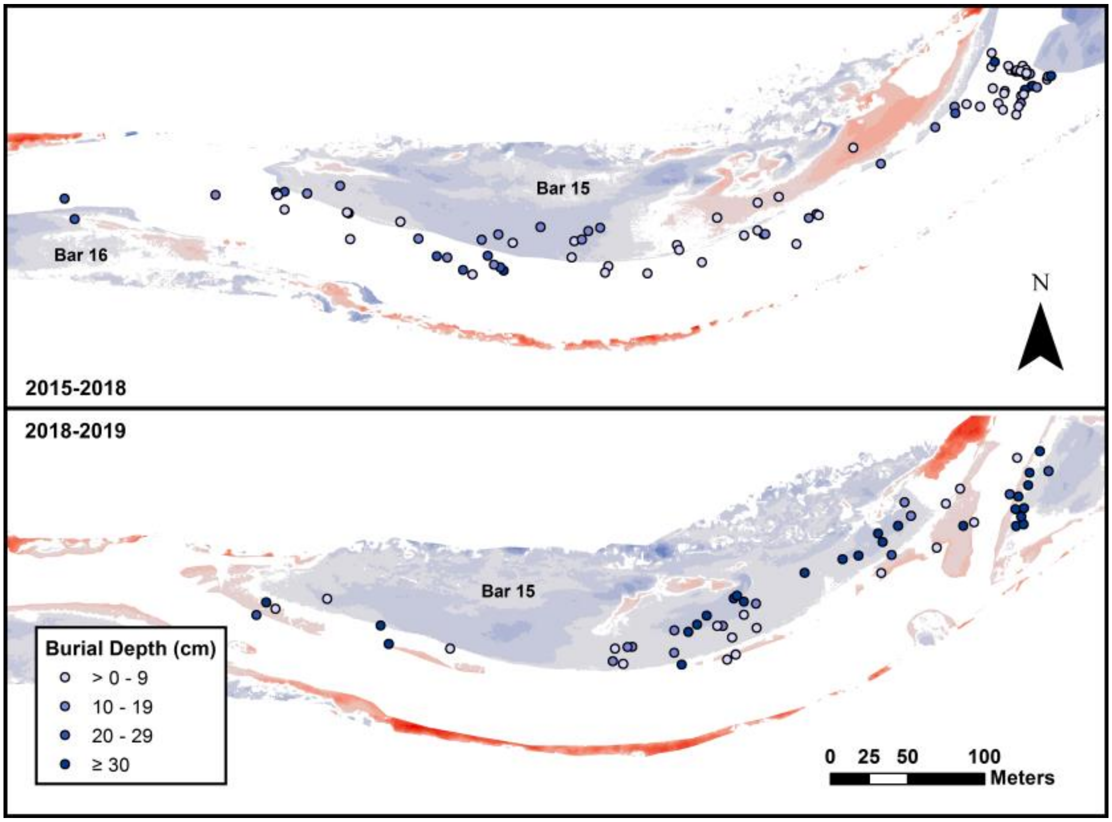

Figure 13. Tracer burial for Bar 15. The position of buried tracers that were recovered between 2015 and 2018 are overlaid on the corresponding DoD in the upper panel. Those recovered in 2019 are shown in the lower panel overtop the 2018-19 DoD.

The distribution of tracer burial depths for Bar 15 is presented in Figure 12c. The median burial depth of 10 cm was the lowest of the three study sites and was also lower than 2 D_{90} for Bar 15 surface sediment (17.7 cm). The lower tracer burial on Bar 15 relative to the other sites aligns with the lower magnitudes of morphologic change observed on DoDs relative to the Bar 6 and Bar 7 reach. Because morphologic change drives burial depth, and local bar dynamics and morphology differ between sites, this produces differences in tracer dispersion and burial between sites. This also means that the distribution of tracer burial depths in this type of channel may not be described by a simple gamma or exponential models as documented in smaller, plane-bed channels (Haschenburger, 2012), but rather that bed particles are irregularly buried at a range of depths related to the location and vertical thickness of erosional and depositional sites.

3.4.3 Summary of morphologic change and particle burial

Between 2015 and 2019, gravel bars on the San Juan River displayed patterns of erosion at the bar head with vertical accretion from the bar apex down to the tail, reflective of downstream bar migration. Lateral accretion was minor at Bars 7 and 15 at or downstream of the bar apex, and most significant on Bar 6. Cut bank retreat was observed at all sites, again, this process was most pronounced opposite Bar 6. The extent of bank erosion is also reflected in the channel sinuosity for each of these reaches, as the channel is most sinuous around Bar 6 and straighter at Bars 7 and 15. Overall, the river displayed lateral instability through migration of bars and cut banks; changes that were generally reflected in patterns of tracer deposition and burial. Tracers seeded on bar tails tended towards immobility or short displacements, due to burial caused by vertical accretion of the bar tail. Of the tracers that travelled longer distances, burial focused at the apex of Bars 6 and 7, and downstream of the apex for Bar 15. Tracer burial depths were typically highest on Bar 6 and lowest on Bar 15, again reflective of the bar dynamics. Overall the spatial patterns of tracer burial were consistent with deposition in DoDs.

3.5 Longer term changes in channel morphology

Channel boundaries were digitized in a GIS using orthophotographs from 1995 to 2019 as well as the Lidar DEMs for 2015, 2018, and 2019 to examine the longer term changes in channel morphology. The mapped channel boundaries over this period for Bars 6, 7, and 15 are presented in Figure 14 along with the 2015-2019 DoDs and positions of buried tracers.

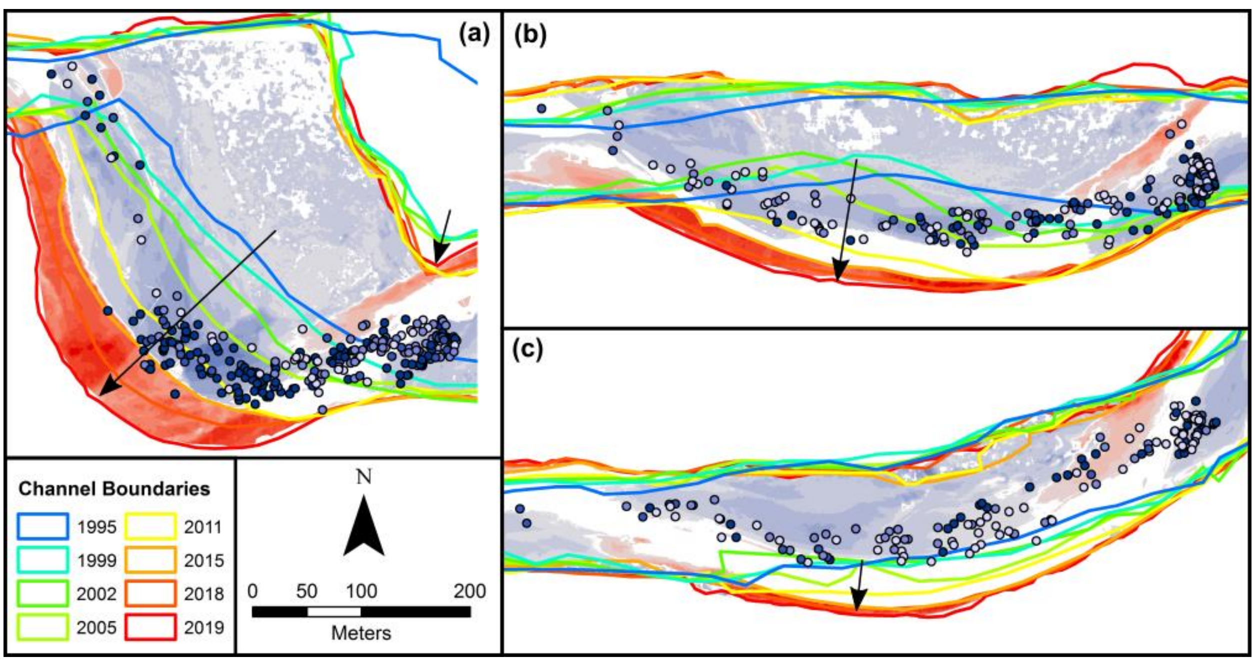

Figure 14. Channel boundaries of the San Juan River from 1995 to 2019 overlaid on top of tracer burial locations and 2015-2019 DoDs for **(a)** Bar 6, **(b)** Bar 7, and **(c)** Bar 15.

Overall, the pattern of particle deposition along the margins of bars, coinciding with the lateral bar accretion and erosion of the cut banks, is reflected in the longer-term changes of the channel boundaries. Since 1995, the channel has widened around each of the three study bars, with the most extreme changes occurring opposite the apex of Bar 6, where the bank has retreated approximately 190 m from 1995 to 2019 (Figure 14a). This aligns with the clustering of tracers deposited at the apex of Bar 6 and high rates of tracer burial in this area. The bank opposite Bar 7 has retreated about 70 m between 1995 and 2019 (Figure 14b). Similar to Bar 6, preferential tracer deposition occurred along the bar margin. Lateral bar accretion occurs opposite the eroding bank; it is unclear which process is independent and which is dependent on the other, or whether the two processes are each dependent on the other process. While bank retreat and lateral bar accretion results in a wider channel, over the long-term the widening is likely offset by revegetation of the less active inner portion of the bars. Ultimately the processes of longer-term channel evolution are reflected in the short-term dynamics of individual bed particle movements.

Of the three sites, Bar 15 has undergone the least substantial changes between 1995 and 2019, with the outer bank retreating about 50 m over this period. This section of channel appears less morphologically active than the other sites, as not only did the 2015-2019 DoD exhibit only minor lateral bar accretion, but tracer burial was also lowest at Bar 15 (Figure 14c). It is possible that the outer bank opposite Bar 15 is more resistant to erosion than the Bar 6 and 7 reach, and therefore morphologic development is different. However, no tests were performed to confirm this. While tracers were still routed along the margin of Bar 15, tracer burial was particularly low, with half of recovered tracers buried less than 10 cm deep. The shallow burial of Bar 15 tracers leaves them more likely to be re-mobilised by future floods and exported out of the area entirely. The Bar 15 reach appears to have less sediment storage and more transfer compared to the Bars 6 and 7 reach.

4 Discussion

The results from particle tracking in the San Juan River reveal insights into bed particle dynamics in a wandering-style gravel-bed river, which has seldom been a focus in previous studies. The recovery rate of tracers in this study is unique for a channel of this size and as such provides important information on the nature of bedload transport in these systems, therefore developing tracer displacement statistics and models for this type of river and relating these to morphologic change and bar development during the four years of tracer deployment.

The intrabedform, or intrabar, transport that was observed on the San Juan River, aligns with results from the few previous bedload tracking results on larger, bar-dominated channels. On the Ain River, France, Rollet et al. (2008) conducted a PIT tag tracer study, recovering 36 % of tracers after one year, with an average travel distance of 50 m, less than one bar length downstream. While interpretation of particle transport was limited by the low recovery rate, the authors noted that over the tracer monitoring period, a thick sedimentary layer had accreted on the edge of the gravel bar immediately downstream of the tracer injection site and posited that lost tracers were likely buried at this location, beyond their antenna's maximum range of detection. This description of bar growth is similar to changes observed on Bar 6 of the San Juan River, where tracer clustering and lateral accretion was focused at the bar apex. In another PIT tag study, conducted on a wandering riffle-pool reach of the Durance River, France, Chapuis et al. (2015) recovered 40 % of tracers after four months, with an average particle path length of 83 m, again indicative of transport within one riffle-pool unit. As observed on the San Juan River, the authors noted that particles deployed on bar tails were either immobile or only displaced short distances, while those seeded closer to the thalweg were transport farther downstream. Similar variations in transport conditions between morphologic units were reported from PIT tag and painted tracer data collect from a wandering reach of the Parma River, Italy (Brenna et al., 2019). The spatial variability in bedload transport, intrinsic to the riffle-pool morphology, means that deployment strategy has a strong influence on tracer mobility and resultant path length distributions. In the cases of the Ain, Durance, and San Juan Rivers, tracers tended to remain within one morphological unit, with minimal transport downstream. This provides direct evidence that in addition to hydraulic controls, channel morphology influences particle dynamics in these systems. Particle trapping and burial in association with bar development appears to be an important consideration in modeling sediment behaviour in this type of river, and therefore in the bedload transport process more generally. This emphasizes the morphologic control on bed particle transport, a point that was also raised in a re-analysis of bedload tracking data by Vázquez-Tarrío et al. (2018).

The pattern of particle displacement and deposition on the San Juan River reflected a combination of morphologic controls and seasonal variations in the flow regime. During the 2017-18 winter, the year with the highest peak discharge and total volume of competent flow, bedload deposition focused at the apex of the first bar downstream, and either slightly positive or symmetrical distributions were observed. However, during years with more moderate floods and lower competent flow volume, path length distributions tended to be positively skewed, with lower tracer mobility. The results from this study provide some validation to the findings from Pyrce and Ashmore's flume experiments (2003a; 2005) whereby they observed bi- and multi-modal path length distributions during bar-forming discharges, with modes coincident with bar apexes.

To further compare tracer transport on the San Juan River with results from the literature, Figure 4 from Vázquez-Tarrío et al. (2018), has been re-created in Figure 15 with data from Bars 6, 7, and 15 on the San Juan River. In this graph, dimensionless stream power (ω^*) was calculated as in Eaton and Church (2011), to compare flow strength and particle transport across rivers of different scales. Mean scaled travel distances were scaled using a morphologic length scale (i.e. the spacing of macroscale bedforms), which for the San Juan River meant the riffle-riffle spacing. Note that only tracers that were recovered after one flood season were used to calculate mean travel distances on the San Juan River, to remove the noise from tracers residing in the channel for multiple flood seasons. Data from the 2015-16 deployment on Bar 6 were not plotted on this graph due to the low recovery rate (33 %) and uncertainty in the statistics of particle displacement for this year.

The San Juan River data appear in line with results from riffle-pool channels, showing a positive relationship between dimensionless stream power and mean scaled travel distance, though travel distances on the San Juan River were relatively low (Figure 15). What is more interesting though, and as noted by Vázquez-Tarrío et al. (2018), is that riffle-pool channels share a common trait in that they rarely exhibit average travel distances beyond 1-2 length-scale units, generally at the lower end of the range for other channel types. It appears that riffle-pool channels have limited transport distances compared with other channels, presumably a result of bars and riffles constraining particle movement. Over the long-term, path lengths are therefore likely to be limited by the rate of bar development and re-working, which in turn plays an important role in overall channel evolution and stability (Reid et al., 2019).

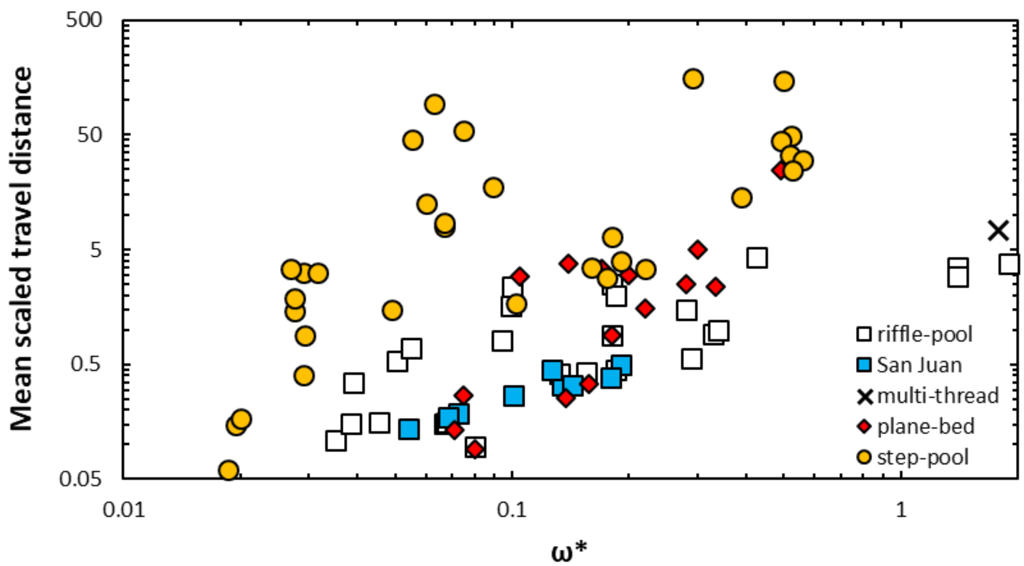

Figure 15. Mean scaled travel distance as a function of dimensionless stream power for various channel types and the San Juan River. This figure is re-created from Figure 4 in Vázquez-Tarrío et al. (2018).

The path length distributions presented in this study reflect particle transport over one to four years. Results between years were similar, providing evidence that the observed patterns of movement and burial are reproducible behaviour. Furthermore, these results likely reflect longer term patterns in bedload transport for the San Juan River. Peak flows were not uncommonly large or small when compared with the historic hydrologic record, so there is no reason to expect anomalous movement due to the magnitude of peak floods. Perhaps more importantly, the preferential deposition and incorporation of tracers in bars has been previously demonstrated to hold true over longer time-scales in gravel-bed rivers in general (e.g. Ferguson et al., 2002; Haschenburger, 2013).

The tracer burial data provide context to the path length analysis and revealed insights into patterns of sediment transfer and storage. Burial depths up to, and likely exceeding, 50 cm were recorded at each of the three sites, although the absolute magnitude of maximum particle burial depth was not obtained in this study due to methodological constraints. However, the development of "wobblestone" technology looks to provide a promising solution to estimating particle burial without the need to physically recover the particles and disturb the bed (Papangelakis et al., 2019). Overall, tracer burial aligned with the patterns of bar-scale deposition observed on DoDs, which raises two important points. First, this suggests that as individual particles are transported to and buried in local areas of deposition, they become incorporated into the channel morphology, and future movement will be limited by the rate of bedform (or bar) migration. This relates back to Neill's (1987) original speculation that over the long term, average particle path lengths may be inferred from the channel morphology. Secondly, the fact that more than 30 % of buried tracers were recovered at depths beyond twice the local D90 for each site suggests that the concept of a shallow active layer less than two particles deep does not reflect the nature of bedload processes occurring in this type of channel. As described by Ashmore et al. (2018), it appears that bed particle deposition and burial in larger, more dynamic rivers is controlled by bar-scale patterns of deposition, whereby the active layer is spatially non-uniform and maximum burial depths occur on the scale of vertical changes in bed level associated with those dominant morphological processes. This is important because the dimensions of the active layer, when combined with the virtual velocity of bed particles, gives the morphological bedload transport rate (Haschenburger and Church, 1998; Mao et al. 2017; Vericat et al., 2017). Tracer burial data for the San Juan River indicate that bedload processes in this type of channel contrast with those in smaller, stable, plane-bed channels, whereby particles move over the surface of the bed with more limited vertical exchange and without significant morphological development and control (Haschenburger, 2012).

5 Conclusion

The primary goal of this study was to investigate the interplay between channel morphology and bed particle displacements in a wandering gravel-bed river channel, and more specifically, to assess whether displacement is tied to bar scale and patterns of bar development and accretion. This has implications for path length when applied to virtual velocity and morphological estimates of bedload and possible differences among rivers of different morphology and size.

Tracers exhibited path length distributions related to morphologic controls (deposition near the bar apex) and differences year to year related to the annual flow regime, with greater dispersion observed during years with greater number of peak floods and flow volume above the threshold discharge for bed mobility. Additionally, tracer deposition and burial were reflected by areas of deposition on DEMs of difference (DoDs). Tracers tended to be deposited along bar margins and to a lesser extent, the surface of the downstream portion of the bars, reflecting the downstream bar migration and lateral bar accretion observed on DoDs and active layer depths greater than that typically assumed in bedload analysis and modeling. This highlights the fundamental importance of bar development and re-working underpinning bedload transport processes in bar-dominated channels and supports recent analyses of morphological effects in tracer dispersion (Vázquez-Tarrío et al., 2018). Ultimately, short-term particle displacements are linked with the morphological style of channel evolution and therefore differs from bedload processes in small, plane-bed channels, for which much previous analysis and theory have been developed.

Acknowledgments, Samples, and Data

This work was funded by the British Columbia Ministry of Forests, Lands, Natural Resource Operations and Rural Development (FLNRORD) and the Pacheedaht First Nation. The data used in this study will be made available through the Western University Dataverse prior to publication (DOI:). We are thankful to Jesse Schafer for preparation of GIS data, and the following persons for their field support: Andrew Boxwell, Spencer Ranson, David Waine, Kyle Fukui, Dave Johnson, Ali Jones, Rachel Dugas, and several FLNRORD employees. We also thank BioMark for their feedback on optimising the RFID antenna setup.

References

Arnaud, F., Piégay, H., Vaudor, L., Bultingaire, L., and Fantino, G. (2015). Technical specifications of low-frequency radio identification bedload tracking from field experiments: Differences in antennas, tags and operators. *Geomorphology, 238*, pp. 37-46.

Arnaud, F., Piégay, H., Béal, D., Collery, P., Vaudor, L., and Rollet, A. (2017). Monitoring gravel augmentation in a large regulated river and implications for process-based restoration. *Earth Surface Processes, 42*, pp. 2147-2166.

Ashmore, P.E., and Church, M. (1998). Sediment transport and river morphology: A paradigm for study. In P.C. Klingeman, R.L. Beschta, P.D. Komar, and J.B. Bradley (Eds.) *Gravel-Bed Rivers in the Environment* (pp. 115-148). Water Resources Publications, LLC, Highland Ranch, Colorado.

Ashmore, P., Peirce, S., and Leduc, P. (2018). Expanding the "active layer": Discussion of Church and Haschenburger (2017) What is the "active layer?" *Water Resources Research* 53, 5-10, Doi:10.1002/2016WR019675. *Water Resources Research, 54*, pp. 1-3.

BC Geological Survey (2018). Bedrock geology [Shapefile]. Retrieved from: https://catalogue.data.gov.bc.ca/dataset/bedrock-geology/resource/aa3a15f8-02fe-49c6-836c-6866c326203d?inner_span=True

Beechie, T.J. (2001). Empirical predictors of annual bed load travel distance, and implications for salmonid habitat restoration and protection. *Earth Surface Processes and Landforms, 26*, pp. 1025-1034.

Bradley, D.N., and Tucker, G.E. (2012). Measuring gravel transport and dispersion in a mountain river using passive radio tracers. *Earth Surface Processes and Landforms, 37*, pp. 1034-1045.

Brasington, J., Langham, J., Rumsby, B. (2003). Methodological sensitivity of morphometric estimates of coarse fluvial sediment transport. *Geomorphology*, *53*, pp. 299-316.

Brenna, A., Surian, N., and Mao, L. (2019). Virtual velocity approach for estimating bed material transport in gravel-bed rivers: Key factors and significance. *Water Resources Research, 55*, pp. 1651-1674.

Cassel, M., Piégay, H., and Lavé, J. (2017). Effects of transport and insertion of radio frequency identification (RFID) transponders on resistance and shape of natural and synthetic pebbles: applications for riverine and coastal bedload tracking. *Earth Surface Processes and Landforms, 42*, pp. 399-413.

Chapuis, M., Bright, C.J., Hufnagel, J., and MacVicar, B. (2014). Detection ranges and uncertainty of passive Radio Frequency Identification (RFID) transponders for sediment tracking in gravel rivers and coastal environments. *Earth Surface Processes and Landforms, 39*(15), pp. 2109-2120.

Chapuis, M., Dufour, S., Provansal, M., Couvert, B., and de Linares, M. (2015). Coupling channel evolution monitoring and RFID tracking in a large, wandering, gravel-bed river: Insights into sediment routing on geomorphic continuity through a riffle-pool sequence. *Geomorphology, 231*, pp. 258-269.

Church, M. (2006). Bed material transport and the morphology of alluvial river channels. *The Annual Review of Earth and Planetary Science, 34*, pp. 325-354.

Church, M., and Ferguson, R.I. (2015). Morphodynamics: Rivers beyond steady state. *Water Resources Research, 51*, pp. 1883-1897.

Church, M., and Hassan, M.A. (1992). Size and distance of travel of unconstrained clasts on a streambed. *Water Resources Research, 28*, pp. 299-303.

Eaton, B., Hassan, M., and Phillips, J. (2008). A Method for Using Magnetic Tracer Stones to Monitor Changes in Stream Channel Dynamics. *Streamline: Watershed Management Bulletin, 12*(1), pp. 22-28.

Eaton, B., and Church, M. (2011). A rational sediment transport scaling relation based on dimensionless stream power. *Earth Surface Processes and Landforms, 37*, pp. 901-910.

Environment and Climate Change Canada (2019). Canadian Climate Normals 1981-2010 Station Data. Retrieved from: http://climate.weather.gc.ca/climate_normals/results_1981_2010_e.html?stnID=82&autofwd=1

Ferguson, R. (2013) Reach-Scale Flow Resistance. *Treatise on Geomorphology, 9*, pp. 50-68.

Ferguson, R.I., Bloomer, D.J., Hoey, T.B., and Werritty, A. (2002). Mobility of river tracer pebbles over different timescales. *Water Resources Research, 38*(5), pp. 3-1 – 3-8.

Haschenburger, J.K. (2012). On gravel exchange in natural channels. In M. Church, P. Biron, and A. Roy (Eds) *Gravel-Bed Rivers: Processes, Tools, Environments* (pp. 56-67). John Wiley, Chichester, UK.

Haschenburger, J.K. (2013). Tracing river gravels: Insights into dispersion from a long-term field experiment. *Geomorphology, 200*, pp. 121-131.

Haschenburger, J.K., and Church, M. (1998). Bed material transport estimated from the virtual velocity of sediment. *Earth Surface Processes and Landforms, 23*, pp. 791-808.

Hassan, M.A., and Bradley, D.N. (2017). Geomorphic controls on tracer particle dispersion in gravel bed rivers. In D. Tsutsumi, and J.B. Laronne (Eds.) *Gravel Bed Rivers: Processes and Disasters, 1* (pp. 159-184). John Wiley & Sons Ltd.

Hassan, M.A., and Roy, A.G. (2016). Coarse particle tracking in fluvial geomorphology. In G.M. Kondolf, and H. Piégay (Eds.) *Tools in Fluvial Geomorphology. Second Edition* (pp. 306-323). Chichester, West Sussex England: Wiley Blackwell.

Hassan, M.A., Church, M., and Ashworth, P.J. (1992). Virtual rate and mean distance of travel of individual clasts in gravel-bed channels. *Earth Surface Processes, 17*, pp. 617 - 627.

Kasprak, A., Wheaton, J.M., Ashmore, P.E., Hensleigh, J.W., and Peirce, S. (2015). The relationship between particle travel distance and channel morphology: Results from physical models of braided rivers. *Journal of Geophysical Research: Earth Surface, 120*, pp. 55-74.

Lamarre, H., MacVicar, B., and Roy, A.G. (2005). Using passive integrated transponders (PIT) tags to investigate sediment transport in gravel-bed rivers. *Journal of Sedimentary Research, 75*, pp. 736-741.

Liébault, F., Bellot, H., Chapuis, M., Klotz, S., and Deschâtres, M. (2012). Bedload tracing in a high-sediment-load mountain stream. *Earth Surface Processes and Landforms, 37*, pp. 385-399.

Mao, L., Picco, L., Lenzi, M.A., and Surian, N. (2017). Bed material transport estimate in large gravel-bed rivers using the virtual velocity approach. *Earth Surface Processes and Landforms, 42*, pp. 595-611.

McQueen, R. (2019). Bed particle displacement in a wandering gravel-bed river. *Electronic Thesis and Dissertation Repository.* 6242. https://ir.lib.uwo.ca/etd/6242

Middleton, L., Ashmore, P., Leduc, P., and Sjogren, D. (2019). Rates of planimetric change in a proglacial gravel-bed braided river: Field measurement and physical modelling. *Earth Surface Processes and Landforms, 44*, pp. 752-765.

Mollard, J.D. (1973). Airphoto interpretation of fluvial features. In *Fluvial processes and sedimentation. National Research Council of Canada, Ottawa, ON* (pp. 341-380). Inland Waters Directorate, Department of the Environment.

Montgomery, D.R., and Buffington, J.M. (1997). Channel-reach morphology in mountain drainage basins. *Geological Society of America Bulletin*, pp. 596 – 611.

Neill, C.R. (1973). Hydraulic and morphologic characteristics of Athabasca River near Fort Assiniboine (pp. 1-23). Alberta Research Council, Edmonton, Highway and River Engineering Division Report REH/73/7.

Neill, C.R. (1987). Sediment balance considerations linking long-term transport and channel processes. In C.R. Thorne, J.C. Bathurst, and R.D. Hey (Eds.) *Sediment Transport in Gravel-Bed Rivers* (pp. 225-239). John Wiley & Sons Ltd.

Northwest Hydraulic Consultants Ltd. (1994). Impact of forest harvesting in terrain stability, stream channel morphology and fisheries resources of the San Juan River Watershed, Vancouver Island. http://a100.gov.bc.ca/pub/acat/public/viewReport.do?reportId=23277

Papangelakis, E., Muirhead, C., Schneider, A., and MacVicar, B. (2019). Synthetic Radio Frequency Identification tracer stones with weighted inner ball for burial depth estimation. *Journal of Hydraulic Engineering*, 145(12), 06019014. https://doi.org/10.1061/(ASCE)HY.1943-7900.0001650

Phillips, C.B., and Jerolmack, D.J. (2014). Dynamics and mechanics of bed-load tracer particles. *Earth Surface Dynamics, 2*, pp. 513-530.

Peirce, S.E.K. (2017). Morphological bedload transport in gravel-bed braided rivers. *Electronic Thesis and Dissertation Repository*. 4595. https://ir.lib.uwo.ca/etd/4595

Pyrce, R.S., and Ashmore, P.E. (2003a). Particle path length distributions in meandering gravel-bed streams: Results from physical models. *Earth Surface Processes and Landforms, 28*, pp. 951-966.

Pyrce, R.S., and Ashmore, P.E. (2003b). The relation between particle path length distributions and channel morphology in gravel-bed streams: a synthesis. *Geomorphology, 56*, pp. 167-187.

Pyrce, R.S., and Ashmore, P.E. (2005). Bedload path length and point bar development in gravel-bed river models. *Sedimentology, 52*, pp. 839-857.

Reid, H.E., Williams, R.D., Brierley, G.J., Coleman, S.E., Lamb, R., Rennie, C.D., and Tancock, M.J. (2019). Geomorphological effectiveness of floods to rework gravel bars: Insight from hyperscale topography and hydraulic monitoring. *Earth Surface Processes and Landforms, 44*, pp. 595-613.

Rollet, A.J., MacVicar, B., Piégay, H., Roy, A.G. (2008). A comparative study on the use of passive integrated transponders to estimate sediment transport: first results (in French). *La Houille Blanche, 4*, pp. 110-116.

Schneider J., Hegglin, R., Meier, S., Turowski, J.M., Nitsche, M., and Rickenmann, D. (2010) Studying sediment transport in mountain rivers by mobile and stationary RFID antennas. In A. Dittrich, K. Koll, J. Aberle, and P. Geisenhainer (Eds.) *River Flow* (pp. 1723-1730). Karlsruhe: Bundesanstalt für Wasserbau. S.

Terra Remote Sensing Inc. (2018a). Project report: Renfrew. September 4, 2018. (pp. 1-29). Sidney, BC.

Terra Remote Sensing Inc. (2018b). Project report: Aerial LiDAR and imagery survey at San Juan River, Vancouver Island, BC. April 24, 2018. (pp. 1-51). Sidney, BC.

Terra Remote Sensing Inc. (2019). Project report: Juan River change detection survey. Port Renfrew, BC. November 12, 2019. (pp. 1-45). Sidney, BC.

Tomsett, C., and Leyland, J. (2019). Remote sensing of river corridors: A review of current trends and future directions. *River Research and Applications*, pp. 1-25.

Vázquez-Tarrío, D., and Batalla, R.J. (2019). Assessing controls on the displacement of tracers in gravel-bed rivers. *Water, 11*, pp. 1-21.

Vázquez-Tarrío, D., Recking, A., Liébault, F., Tal, M., and Menéndez-Duarte, R. (2018). Particle transport in gravel-bed rivers: Revisiting passive tracer data. Earth Surface Processes and Landforms, 44, pp. 112-128.

Vericat, D., Wheaton, J.M., and Brasington, J. (2017). Revisiting the morphological approach. In D. Tsutsumi and J.B. Laronne (Eds.) *Gravel Bed Rivers: Processes and Disasters, 1* (pp. 121-158). John Wiley & Sons Ltd.

Water Survey of Canada (2019). Monthly Discharge Data for SAN JUAN RIVER NEAR PORT RENFREW (O8HA010) [BC]. Retrieved from: https://wateroffice.ec.gc.ca/report/historical_e.html?stn=08HA010&mode=Table&type=h2oArc&results_type=historical&dataType=Monthly&parameterType=Flow&year=2017&y1Max=1&y1Min=1

Wheaton, J.M., Brasington, J., Darby, S.E., and Sear, D.A. (2010). Accounting for uncertainty in DEMs from repeat topographic surveys: improved sediment budgets. *Earth Surface Processes and Landforms, 35*, pp. 135-156.

Wilcock, P.R. (1997). Entrainment, displacement and transport of tracer gravels. *Earth Surface Processes and Landforms, 22*, pp. 1125 - 1138.

Wolman, M.G. (1954). A method of sampling coarse river-bed material. *Transactions, American Geophysical Union, 35*(6), pp. 951-956.